Reaction Kinetics, Mechanisms and Catalysis (2018) 125:675–688
https://doi.org/10.1007/s11144-018-1477-y

Impact of chloride ions on the oxidative coupling of methane over Li/SnO_2 catalyst

Fei Cheng[1,2] · Jian Yang[1] · Liang Yan[1] · Jun Zhao[1] · Huahua Zhao[1] · Huanling Song[1] · Lingjun Chou[1,3]

Received: 21 May 2018 / Accepted: 25 September 2018 / Published online: 11 October 2018

Abstract

The catalytic performance for the oxidative coupling of methane (OCM) over chloride-containing Li/SnO_2 was investigated experimentally and the mechanism of OCM was further suggested. Cl^- ions exerted remarkable influence on the catalytic performance of Li/SnO_2, with that at 750 °C displaying the highest catalytic activity (18.5% C_2 yield) for OCM. The prepared catalysts were characterized with N_2 physisorption, X-ray diffraction, O_2-temperature programmed desorption, X-ray photoelectron spectroscopy and H_2 temperature programmed reduction measurement to elucidate the effect of Cl^- ions on its properties and catalytic performance. The results showed that the enhanced OCM catalytic activity of the chloride-containing Li/SnO_2 catalysts compared with pure Li/SnO_2 catalyst may originate from the higher concentration of anion vacancies, more rapid oxygen mobility and improved redox ability of tin. In addition, characterization by CO_2-temperature programmed desorption, infrared spectroscopy and O_2 frequency pulse reactions results illustrated that adding Cl^- ions improved performance of Li/SnO_2, which not only reduced strong basic sites to prevent the formation of poisoning carbonate, but also facilitated the formed chloromethane to convert quickly to ethylene.

Keywords OCM · Active oxygen · Chloride-containing · Lithium oxide · Pulse reaction

Electronic supplementary material The online version of this article (https://doi.org/10.1007/s11144-018-1477-y) contains supplementary material, which is available to authorized users.

✉ Lingjun Chou
ljchou@licp.cas.cn

[1] State Key Laboratory for Oxo Synthesis and Selective Oxidation, Lanzhou Institute of Chemical Physics, Chinese Academy of Sciences, Lanzhou 730000, People's Republic of China

[2] University of Chinese Academy of Sciences, Beijing 100049, People's Republic of China

[3] Suzhou Research Institute of LICP, Chinese Academy of Sciences, Suzhou 215123, People's Republic of China

Introduction

The oxidative coupling of methane (OCM) is considered as a promising potential one-step process for the production of useful basic petrochemicals (ethylene, ethane) from methane, which has been intensively investigated since the early work of Keller and Bhasin [1]. Up to date, a large number of composites have been tried as catalysts for OCM [2–8].

Tin oxide (SnO_2) which remains widely used in practice is excellent catalyst support [9–11], primarily due to its high adsorption capacity, high temperature resistant, wide band gap and mechanic stability. Moreover, Sn is found to prevent the evaporation of lithium, improving the stability through the generation of complex oxides [12, 13].

The chloride-containing lithium oxides have so far been found to be effective in catalyzing the OCM. According to a considerable number of studies [14, 15], the chloride-containing lithium oxide catalysts supported on metal oxides caused an increase in methane conversion, yield and total selectivity of C_2 hydrocarbons. In some cases, a direct correlation between the Cl^- ions and the catalytic activity was observed. In some other cases, however, the relationship between the Cl^- ions and catalytic activity was shown to be rather ambiguous. Although a number of investigations [16–18] in the OCM process are tested on the chloride-containing catalysts, not much attention have been given by researchers to the changes in the structures, morphologies and properties of the catalyst surface. Hence, there are still some controversies as to the role of their structures, oxygen mobility, active oxygen, basicity and redox ability in creating their own catalytic effectiveness and the performance of the catalysts containing Cl^- ions.

Here, we report the application of chloride and lithium modified SnO_2 as catalyst for the OCM reaction and the catalyst system was found to be excellent candidates for C_2 formation. The characteristics of the pathway for the formation of C_2 and the method including critical factors were discussed. We also reported how we came to and consequently characterized the chloride-containing lithium-doped SnO_2 catalyst using techniques such as N_2 physisorption, X-ray diffraction (XRD), CO_2-temperature programmed desorption (CO_2-TPD), O_2-temperature programmed desorption (O_2-TPD), X-ray photoelectron spectroscopy (XPS), H_2-temperature programmed reduction measurement (H_2-TPR), infrared spectroscopy (FT-IR) and mass spectrometry (MS). The aim of the study was to find out the role of chloride ions addition to Li/SnO_2 catalysts in the OCM process, as well as to concentrate our attention on the oxidant activation process over catalyst surface.

Experimental

Catalysts synthesis

Chloride-containing Li/SnO_2 catalysts were prepared from tin(II) chloride dihydrate ($SnCl_2{\cdot}2H_2O$, Shanghai Reagent Factory) and lithiumnitrate ($LiNO_3$, Sichuan Longxi Chemical Co., Ltd.). A certain amount of $SnCl_2{\cdot}2H_2O$ was dissolved in

100 mL distilled water under constant stirring and the pH was adjusted to about 2 by adding ammonia water. An aging treatment process was undertaken at room temperature for 5 h. Then the obtained mixture was washed with distilled water (50 ml) with different times (0, 1, 3 and 20 times) to obtain the precursors with different chlorine contents. Then the precursors were dried in an oven with a temperature of 80 °C. The catalysts were obtained through a wet impregnation of the chloride-containing SnO_2 with a lithiumnitrate solution. After drying at 80 °C overnight, the catalyst was calcinated at 800 °C for 3 h. The catalysts with different surface chloride contents were denoted as Li/SnO_2(x) (wt(Li) = 10%, x stands for Cl/Li atomic ratio). X (x stands for Cl/Li atomic ratio of sample) was 0.7, 0.5, 0.2 and 0 when the washing times of the precursors were 0, 1, 3, and 20, respectively. The Li/SnO_2(0.5) after 14 h of the OCM reaction were denoted as Li/SnO_2(spent), where spent represents the Cl/Li atomic ratio was 0.02. The Cl/Li atomic ratio determined by XPS.

Catalytic activity

OCM reaction was carried out with catalyst (0.20 g, 40–60 mesh) at atmospheric pressure in a quartz fixed bed system (I.d. 10 mm). In all experiments, CH_4 and O_2 (2.5:1) were passed through the reactor and the gas hourly space velocity (GHSV) was 7200 h^{-1} during the OCM reaction. The reaction temperature was measured by a thermocouple inserted outside of the quartz reactor. The effluent gases were analyzed on-line by the gas chromatography equipped with a hydrogen flame ionization detector (FID) and a thermal conductivity detector (TCD). The conversion of methane and the selectivity were calculated based on the balance of carbon (100 ± 2%). All the data were obtained after 30 min reaction.

O_2 frequency pulse reactions were performed using the U-shaped quartz reactor over the series catalysts. The catalyst was heated in methane atmosphere (99.99%, 7.1 mL·min^{-1}) to the temperature of 750 °C for 40 min and then the different frequency pulse of O_2 was introduced. The time intervals of O_2 pulses were varied from 15 to 300 s. The reaction products were monitored with an LC-D200 M quadruple mass spectrometer (MS, TILON).

Catalyst characterization

XRD patterns were recorded on an X'Pert Pro Multipurpose diffractometer (PANalytical, Inc.) using the Ni-filtered Cu K_α radiation (0.15406 nm) from 10.0° to 80.0°.

The N_2 adsorption–desorption isotherms were carried out on an Autosorb-iQ analyzer (Quantachrome Instruments U.S.). Prior to the measurements, all the catalyst samples were outgassed at 200 °C for 4 h. The specific surface areas were calculated via the Brunauer–Emmett–Teller (BET) method in the relative pressure ranging from 0.05 to 0.3. Pore size distributions were calculated by the Barrett–Joyner–Halenda (BJH) method from the adsorption isotherms of the samples.

CO_2-TPD, O_2-TPD and H_2-TPR were all performed on an Autosorb-iQ analyzer (Quantachrome Instruments U.S.).

The CO_2-TPD analysis was carried out as follows: The calcined catalyst sample (150 mg) was first treated with He stream (30 mL/min) at 300 °C for 1 h to remove adsorbed impurities. After cooling to room temperature, CO_2 (30 mL/min) was adsorbed on the catalyst sample for 1 h. Finally, the sample was heated from room temperature to 980 °C at a heating rate of 10 °C/min in He gas (30 mL/min) to proceed the CO_2-TPD and CO_2 consumption was measured by a TCD.

The O_2-TPD analysis was carried out as follows: The sample (100 mg) was first treated with He stream (30 mL/min) at 500 °C for 1 h to remove adsorbed impurities. After cooling to room temperature, the catalyst sample was exposed to O_2 stream (30 mL/min) for 1 h. Finally, the sample was heated from room temperature to 980 °C at a heating rate of 20 °C/min in He gas (30 mL/min) to proceed the O_2-TPD and O_2 consumption was measured by a TCD.

The H_2-TPR analysis was carried out as follows: The sample (10 mg) was first treated with Ar stream (40 mL/min) at 300 °C for 1 h to remove adsorbed impurities. After cooling to 40 °C, the H_2 (40 mL/min) was adsorbed on the catalyst sample for 30 min. Finally, the sample was heated from room temperature to 980 °C at a heating rate of 20 °C/min in a flowing H_2 gas (30 mL/min) to proceed the H_2-TPR and H_2 consumption was measured by a TCD.

XPS analyses were carried out with a Thermo Fisher Scientific ESCALAB250xi spectrometer with Mg Kα radiation.

FT-IR spectra were recorded from 400 to 4000 cm^{-1} on a TENSOR27 FTIR spectrophotometer (Bruker).

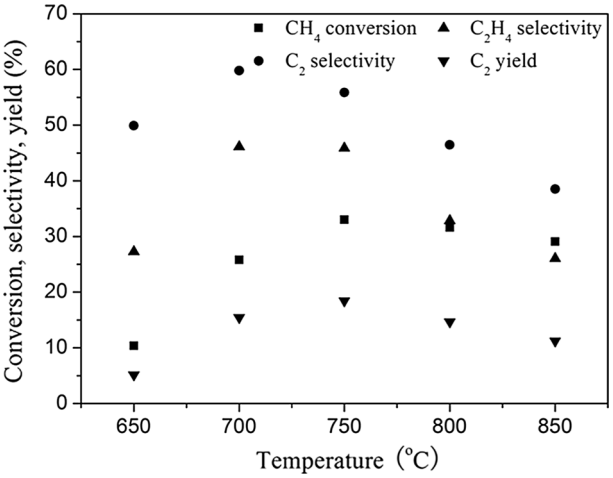

Fig. 1 Comparison of the catalytic performance of $Li/SnO_2(0.5)$ catalysts at different reaction temperature. Reaction conditions: CH_4/O_2 = 2.5, GHSV = 7200 ml/(h g), 0.20 g catalyst

Results and discussion

Comparison of performance of catalysts

Fig. 1 shows the results of OCM reactions over Li/SnO_2(0.5) catalyst at different reaction temperatures. CH_4 conversion and C_2H_4 selectivity suffered a serious decrease at the temperature from 750 to 800 °C. It indicated that some surface active sites benefiting the C_2 and C_2H_4 selectivity were not stable at temperature above 750 °C. Raising the reaction temperature up to 750 °C, the maximum C_2 yield of 18.5% was obtained with the CH_4 conversion of 33.0% and C_2 selectivity of 55.9%, had an overall beneficial effect on the catalytic capability of the Li/SnO_2(0.5) catalyst. However, the CH_4 conversion and C_2 selectivity decayed gradually at even higher temperatures because of the complete oxygen conversion and non-oxidative side reactions.

Fig. 2 shows the results of OCM reactions over Li/SnO_2 catalysts with various Cl/Li atomic ratios. Compared with the Li/SnO_2(0) catalyst, the addition of Cl^- ions significantly improved the CH_4 conversion, C_2 selectivity, C_2H_4 selectivity and C_2 yield over all the chloride-containing Li/SnO_2 at 750 °C. It suggested that high activity for OCM of the chloride-containing Li/SnO_2 catalysts should be ascribed to the addition of Cl^- ions. Comparable results have been obtained for the OCM reaction where the C_2 yield reached a maximum value (18.5%) at a nominal ratio of Cl/Li = 0.5. The C_2 yield decreased from its maximum as Cl/Li atomic ratios increased to 0.7. This result suggested that excessive chloride ions were certainly unfavorable.

To study the performance of Li/SnO_2 during long-term use, the Li/SnO_2(0.5) were selected as representative for catalysts under the optimal conditions. It can be found from Fig. 3 that the performance of Li/SnO_2(0.5) decreased remarkably after 14 h of the OCM reaction. Decreasing chlorine content of the catalyst after the

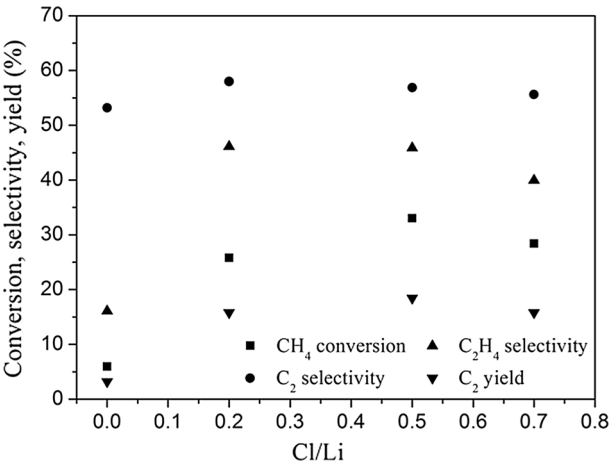

Fig. 2 Comparison of the catalytic performance of Li/SnO_2 catalysts with various Cl/Li atomic ratios at 750 °C. Reaction conditions: CH_4/O_2 = 2.5, GHSV = 7200 ml/(h g), 0.20 g catalyst

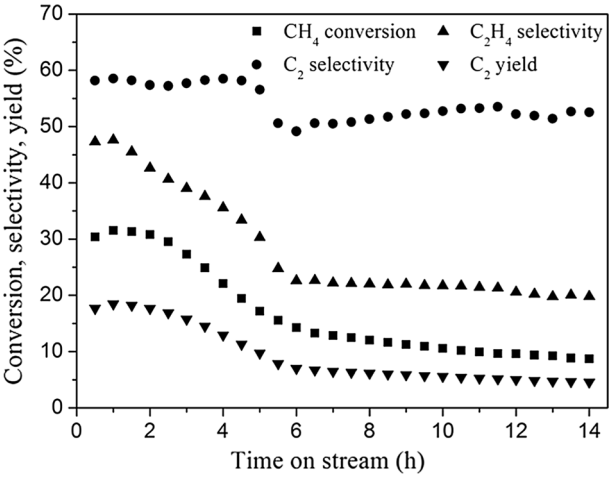

Fig. 3 Long term stability test over $Li/SnO_2(0.5)$ catalyst. Reaction conditions: $CH_4/O_2 = 2.5$, GHSV = 7200 ml/(h g), 0.20 g catalyst

OCM reaction had been reported in previous studies [13]. It was generally suggested that the reduction on the catalytic performance contributed to the loss of chlorine from the chloride-containing Li/SnO_2. This was also in good agreement with the above-mentioned XPS results. It was particularly noted that the C_2H_4 selectivity drastically decreased while the C_2 selectivity decreased slightly. The result indicated that OCM reaction involving chlorine were largely responsible for ethylene formation on chloride-containing Li/SnO_2 and would be further evidenced by O_2 frequency pulse reaction.

Catalyst characterization

The BET specific surface area and surface composition of a series of catalysts are given in Table 1. It should be noted that all catalysts were provided with low specific surface area low to 3.0 m^2/g, and narrow average pore size in a small range of 3.1–3.4 nm. For Li/SnO_2 catalyst, the BET specific surface area increased from 3.0 to 5.1 m^2/g when the Cl/Li atomic ratios increased. Thus, lithium promoted sintering of the SnO_2, while chloride ions inhibited this effect [16]. Comparing the

Table 1 The specific BET surface area and pore size of Li/SnO_2 catalyst

Catalyst	BET specific surface area ($m^2 \cdot g^{-1}$)	Pore size (nm)
SnO_2	10.7	3.1
$Li/SnO_2(0)$	3.0	3.1
$Li/SnO_2(0.2)$	3.4	3.4
$Li/SnO_2(0.5)$	4.9	3.1
$Li/SnO_2(0.7)$	5.1	3.4
Li/SnO_2(spent)	3.5	3.1

data in Table 1, the specific surface areas of the Chloride-containing Li/SnO_2 catalysts were higher than $Li/SnO_2(0)$, this might be beneficial for improving the OCM catalytic activity of the Li/SnO_2 catalyst [19]. After OCM reaction, Li/SnO2(spent) was 3.5 m^2/g, indicating that the specific surface areas of the catalyst reduced during OCM reactions. However, these low specific surface areas, typical for most of the OCM catalysts, seemed not having a determinant effect on the OCM catalytic behavior.

Fig. 4 shows the XRD patterns of Li/SnO_2 catalysts with various Cl/Li atomic ratios. The XRD results confirmed that two different phases, i.e. the tetragonal SnO_2 (JCPDS No. 88-0287) and the Li_2SnO_3 (JCPDS No. 31-0761), co-existed in the product. It was noticeable that the diffraction peaks of $2\theta = 18°$ shifted to lower angle with increasing Cl/Li atomic ratios, which implied lattice expansion. The lattice expansion might be owing to the replacement of the O^{2-} (R = 1.4 Å) sites by Cl^- (R = 1.81 Å) ions. With the Cl/Li atomic ratio was increased to more than 0.2, the diffraction intensity of SnO_2 phase increased and a novel phase of LiCl (JCPDS No. 02-0640) accompanied by the reduction of Li_2SnO_3 phase. It demonstrates clearly that Cl^- ions had been doped into the matrix of Li_2SnO_3 in the samples to destroy the structure of Li_2SnO_3 to form SnO_2 and LiCl. XRD results showed almost identical phases of $Li/SnO_2(0.5)$ and Li/SnO_2(spent), indicating that the loss of chlorine did not remarkably influence the catalyst structure. Furthermore, the diffraction peaks ($2\theta = 18°$) of Li/SnO_2(spent) shifted very slightly compared with the $Li/SnO_2(0.5)$. Reduction of Sn^{4+} [Sn^{4+} (R = 0.69 Å) and Sn^{2+} (R = 1.12 Å)] partly occurred after the OCM reaction as evidenced from the increase of the Sn^{2+}/Sn^{4+} atomic ratio compared to $Li/SnO_2(0.5)$ (Supplementary XPS spectra of Sn $3d_{5/2}$).

Fig. 5 shows the CO_2-TPD patterns of Li/SnO_2 catalysts with various Cl/Li atomic ratios. The desorption temperature centered at 200 °C was assigned to the

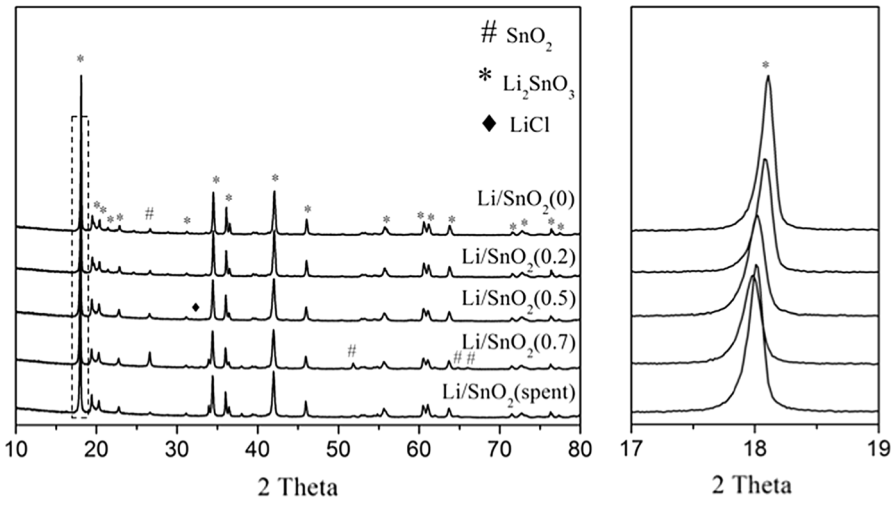

Fig. 4 XRD Pattern of $Li/SnO_2(x)$

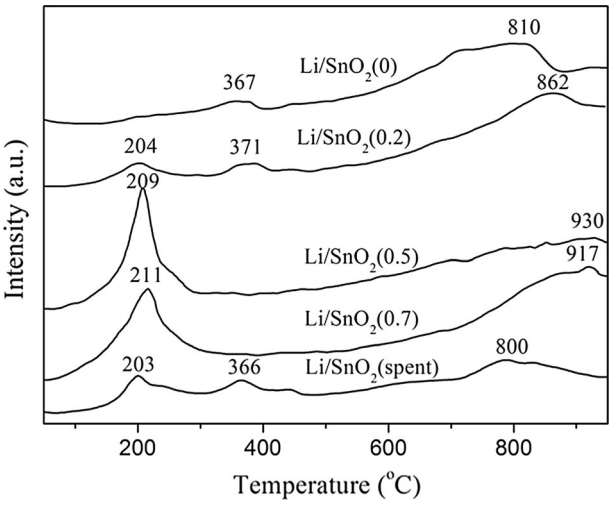

Fig. 5 CO_2-TPD patterns of $Li/SnO_2(x)$

weak basic site, and the desorption range from 300 to 600 °C attributed to the medium basic site, and desorption range above 600 °C corresponded to the strong basic site [20]. The distinct difference of basic sites on the catalyst surfaces was one of the reasons for catalytic behavior of the Li/SnO_2 catalysts for OCM reaction [21]. With the introduction of chloride content, the weak basic sites increased, resulted in the improvement on the capability of catalyst to absorb O_2 and CH_4. Moreover, the addition of chloride could be of advantage for OCM, which reduced strong basic sites to prevent the formation of poisoning carbonate [22]. Moreover, after OCM reaction, the Li/SnO_2(spent) catalyst exhibited a profile very different to that of the fresh $Li/SnO_2(0.5)$ catalyst: there were smaller CO_2 desorption peaks at 209 °C and larger desorption above 600 °C. This result further highlighted that the introduction of chloride content could increase weak basic sites and reduce strong basic sites.

To reveal the surface oxygen properties of catalysts, the O_2-TPD of Li/SnO_2 catalysts with various Cl/Li atomic ratios are recorded in Fig. 6. The samples presented two distinct desorption peaks, one below 500 °C and one above 800 °C, corresponding to the release of adsorbed oxygen and lattice oxygen (O^{2-}) [23, 24], respectively. No obvious desorption peak (< 500 °C) was apparent for the $Li/SnO_2(0)$ as it likely possessed few chemisorbed oxygen on the surface. The chloride-containing Li/SnO_2 possessed obvious desorption peak below 500 °C implying that the incorporation of Cl^- ions is favorable for the oxygen adsorption and activation, consequently promoting the catalytic performance of chloride-containing Li/SnO_2 for OCM [25–28]. As for the chloride-containing Li/SnO_2, Cl^- ions doped into the crystal lattice of Li_2SnO_3 occupied the O^{2-}, the generation of anion vacancies is inevitably promoted, which available to oxygen adsorption and activation [29]. On comparing all the chloride-containing Li/SnO_2, $Li/SnO_2(0.7)$ exerted a smaller desorption peak (< 500 °C). The result demonstrated that excessive Cl^- ions were unavailable to adsorb oxygen because the surface of

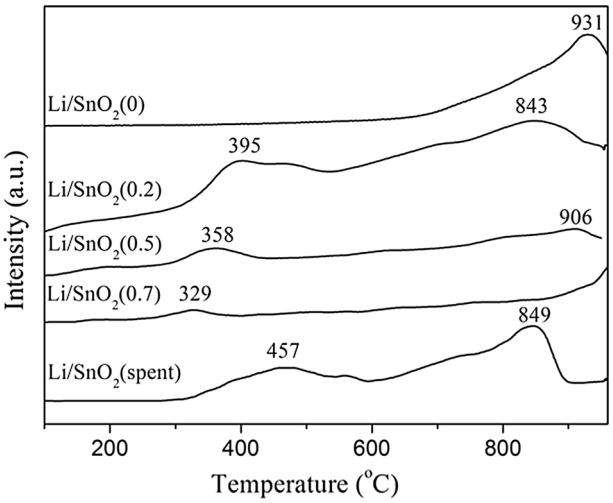

Fig. 6 O_2-TPD patterns of Li/SnO_2(x)

catalyst was covered with a large number of LiCl, which had relatively poor adsorption capacities for oxygen. Besides, the Li/SnO_2 catalyst showed a shift in the lattice oxygen (O^{2-}) peak to a lower temperature with the increase of Cl/Li atomic ratios, which would indicate that the mobility of lattice oxygen (O^{2-}) species were improved. Meanwhile, the highest lattice oxygen (O^{2-}) desorption temperature was observed on the Li/SnO_2(0.7) catalyst had been attributed to too much surface lattice oxygen (O^{2-}) occupied by Cl^- ions. After 14 h of OCM reaction, the O_2-TPD profile of Li/SnO_2(spent) showed two peaks at 457 and 849 °C. The correlation of the O_2-TPD profile of used and fresh Li/SnO_2 further testified that addition Cl^- ions were benefit to generate active oxygen and promoted the oxygen mobility.

Fig. 7 shows the XPS spectra of O1 s for Li/SnO_2 catalysts with various Cl/Li atomic ratios. The O1 s spectra of each catalyst can be attributed to four peaks corresponding to three types of oxygen species: lattice oxygen (O^{2-}, 530.2 eV), chemisorbed oxygen (O_2^{2-} or O^-, 531.1 eV and O_2^-, 532.3 eV) and carbonate groups (533.2 eV) [30–34]. Apparently, the value of (O_2^- + O_2^{2-} or O^-)/O^{2-} of chloride-containing Li/SnO_2 was higher than that of Li/SnO_2(0) (Supplementary Table S1). It has been widely reported that chemisorbed oxygen (O_2^-, O_2^{2-} or O^-) was the most active oxygen for OCM [35–37]. Therefore, the activity of chloride-containing Li/SnO_2 was found to be higher than Li/SnO_2(0). It was commonly accepted that lattice oxygen (O^{2-}) was responsible for abstracting hydrogen from C_2H_6 to form C_2H_4 and chemisorbed oxygen (O_2^-, O_2^{2-} or O^-) were effective for the oxidation reaction [25, 28, 38, 39]. More importantly, the O_2^- ion is thermally stable only below 750 °C [40]. Therefore, taking into consideration of the above factors, CH_4 conversion and C_2H_4 selectivity suffered the serious decrease with increasing the temperature from 750 to 800 °C, which was in good agreement with the experimental results (Fig. 1). As shown in Fig. 2, the C_2H_4 selectivity decreased with increasing chloride content, which could be due to the O^{2-} content reduction.

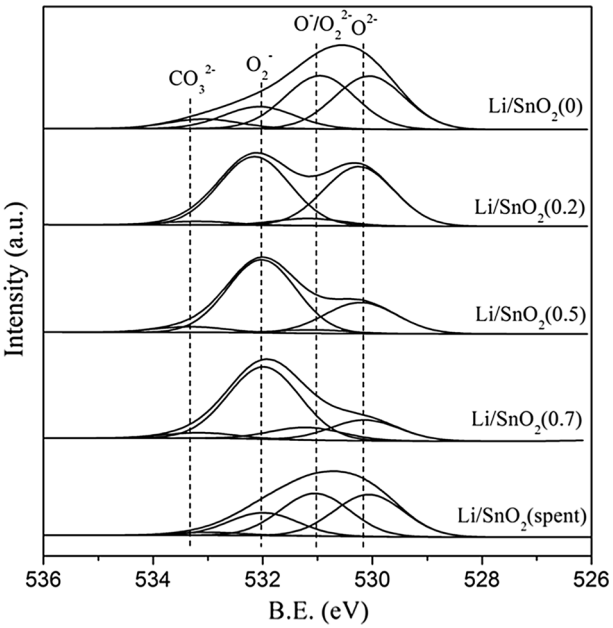

Fig. 7 XPS spectra for O1s of $Li/SnO_2(x)$

This indicated that the Cl^- ions had entered into the positions previously by lattice oxygen (O^{2-}) [41], consistent with the results of O_2-TPD. An appropriate amount of Cl^- ions doping could enhance the OCM activity of Li/SnO_2, which resulted from a synergistic effect of lattice oxygen (O^{2-}) and chemisorbed oxygen (O_2^-, O_2^{2-} or O^-) of catalyst. As a comparison, the value of ($O_2^- + O_2^{2-}$ or O^-)/O^{2-} of chloride-containing Li/SnO_2 was higher than that of Li/SnO_2(spent), indicating that the loss of Cl^- ions during the OCM reaction took place. It seemed certain that the value of ($O_2^- + O_2^{2-}$ or O^-)/O^{2-} was associated with the chlorine content.

As shown in Fig. 8, the Sn $3d_{5/2}$ peaks can be deconvoluted into two peaks to Sn^{2+} (486.1 eV) and Sn^{4+} (486.7 eV) species [42]. It was evident that the addition of Cl^- ions into the Li/SnO_2 led to a significant increase of the Sn^{2+}/Sn^{4+} atomic ratio compared to $Li/SnO_2(0)$. This demonstrated that Sn^{2+} was formed by an electron transfer from the O^{2-} to Sn^{4+}, increased the mobility of oxygen. After 14 h of OCM reaction, the Sn^{2+}/Sn^{4+} atomic ratio of Li/SnO_2(spent) appeared to be higher than obtained over $Li/SnO_2(0.5)$. The result implied that Sn^{4+} was reduced in the course of the OCM reaction.

FT-IR spectra can provide information on the chemical structure of catalyst materials. To reveal the surface functional groups of catalysts, the FT-IR spectra of Li/SnO_2 catalysts with various Cl/Li atomic ratios were recorded. Fig. 9 shows the obtained FT-IR spectra in the region 1300–1800 cm^{-1}. FT-IR bands of surface carbonate species were observed at 1438 and 1510 cm^{-1} [43]. It showed that the addition of appropriate chloride content can significantly prevent the formation of poisoning carbonate, with $Li/SnO_2(0.5)$ displaying the highest performance [44].

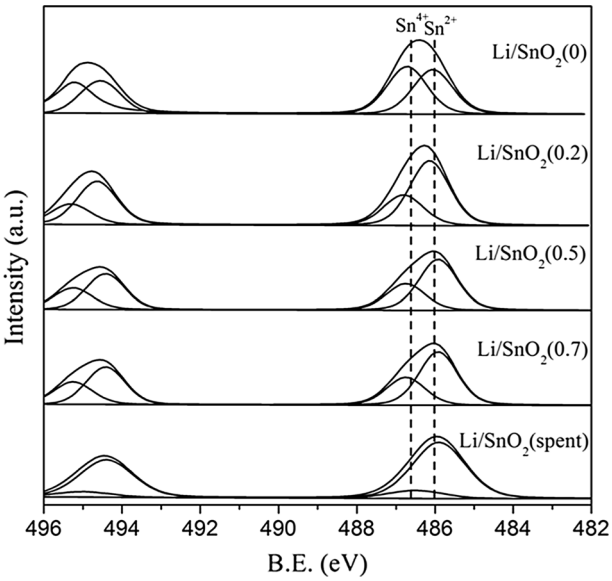

Fig. 8 XPS spectra for Sn 3d of $Li/SnO_2(x)$

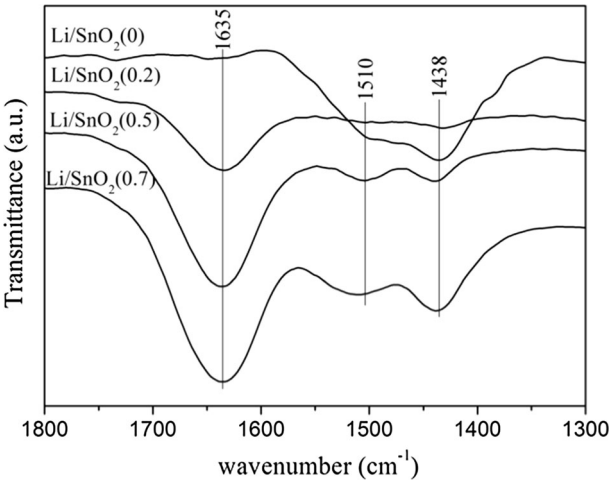

Fig. 9 FT-IR spectra of $Li/SnO_2(x)$

The result might indicate that the addition of appropriate amount chloride decrease the amount of adsorbed CO_2, which was in agreement with the results obtained from CO_2-TPD experiments. In the case of chloride-containing Li/SnO_2, the intensive peak centered at 1635 cm^{-1} might be attributed to the presence of LiCl.

H_2-TPR profiles of Li/SnO_2 catalysts with various Cl/Li atomic ratios are shown in Fig. 10. The TPR profiles of all catalysts show two reduction peaks in the regions of 470–620 and 620–700 °C, respectively. The clear reduction at lower temperature

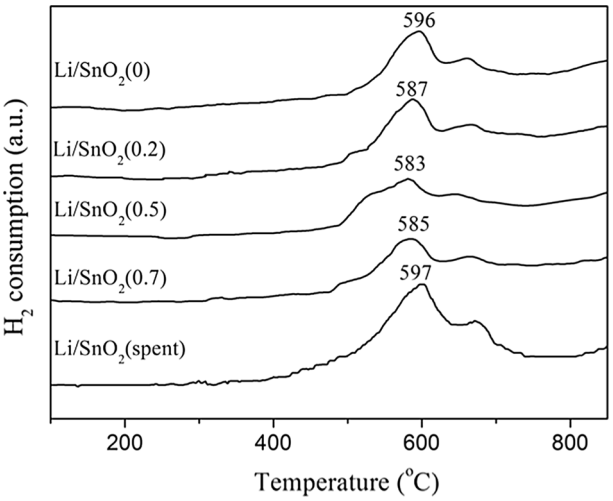

Fig. 10 H_2-TPR patterns of $Li/SnO_2(x)$

(470–620 °C) may be attributed to the reduction of Sn^{4+} to Sn^{2+}. The weak reduction at higher temperature could be ascribed to the reduction of Sn^{2+} to metallic Sn^0 [45]. It was particularly noted that Sn^{4+} reduction peak shifts to lower temperature with the increase of Cl/Li atomic ratios, suggestive of the incorporation of Cl^- ions was beneficial to oxygen mobility [46–49]. The incorporation of Cl^- ions produced higher concentration of anion vacancies, which increases their capability to trap more electrons [50]. Therefore, Cl^- ions was incorporated into the structure of Li_2SnO_3, explaining the relatively low reduction temperature. It was clear that the loss of Cl^- ions was occurring during the OCM reactions because the reduction peaks of Li/SnO_2(spent) were found to shift to higher temperature after the OCM reactions. This further proved that the introduction of chloride content could promote the reduction of Sn^{4+}.

To gain insight into the chlorine behavior of the reaction products, O_2 frequency pulse reaction on chloride-containing Li/SnO_2 was carried out. Fig. S1 shows the mass spectrum signals of O_2 (m/z = 32), C_2H_4 (m/z = 27 for C_2H_4 instead of m/z = 28 to avoid interference caused by CO_2) and CH_3Cl (m/z = 50) for the pulse reaction of O_2 over Li/SnO_2 catalysts at 750 °C. Only C_2H_4 was produced over the $Li/SnO_2(0)$ catalyst. However, both CH_3Cl and C_2H_4 signals were observed over the chloride-containing Li/SnO_2. With the introduction of oxygen, the CH_3Cl and C_2H_4 signals increased rapidly and tended to a relatively steady level. Besides, the CH_3Cl can convert to ethylene in the gas phase [51]. Therefore, taking into consideration all the factors, the slight decrease in C_2H_4 selectivity with decreasing the CH_3Cl, which was in good agreement with the experimental results (Fig. S1). This result can be inferred that the reaction of methane and Cl^- ions over the chloride-containing Li/SnO_2 proceeds to a considerable extent. We assumed that in OCM experiments, radical reactions involving chlorine are largely responsible for

ethylene formation on chloride-containing Li/SnO_2. A possible reaction path for the formation of ethylene in the OCM may be proposed from these findings:

$$CH_4 + Cl^- + 1/2O_2 \rightarrow CH_3Cl + OH^- \quad (1)$$

$$2CH_3Cl \rightarrow C_2H_4 + 2HCl \quad (2)$$

Reaction 1 may take place on chloride-containing Li/SnO_2 and then chloromethane quantitatively converted to ethylene in the gas phase. Moreover, it was noted that the loss of chlorine from the catalyst is associated with HCl production.

Before the introduction of O_2, the catalyst was pretreated with methane at 750 °C for 40 min in order to remove oxygen species on the catalyst surface. As shown in Fig. S1, the O_2 signals over chloride-containing Li/SnO_2 samples were much weakened compared to those over the $Li/SnO_2(0)$, indicating that the additive of Cl^- ions was available to adsorb and activate oxygen to generate active oxygen and promote oxygen mobility.

Conclusions

A series of chloride-containing Li/SnO_2 were prepared which are capable of selectively converting methane to C_2 and higher hydrocarbons at 750 °C. At the nominal ratio of Cl/Li = 0.5, 7200 ml/(h g) GHSV and 0.20 g catalyst, the highest C_2 yield of 18.5% was achieved with the CH_4 conversion of 33.0% and C_2 selectivity of 55.9%. The influence of Cl^- doping on the structures of Li/SnO_2 was investigated. When incorporated Cl^- content, the Cl^- ions doped into the crystal lattice of Li_2SnO_3 or SnO_2 and occupy the O^{2-}, the generation of anion vacancies was inevitably promoted, which had strong tendency to adsorb and activate oxygen to generate active oxygen (O_2^-, O_2^{2-}or O^-) and promoted the oxygen mobility. Adding Cl^- ions improved performance of Li/SnO_2, which not only reduced strong basic sites to prevent the formation of poisoning carbonate and shifted to weak basic sites became beneficial to absorb O_2 and CH_4, but also facilitated excellent redox ability to promote the catalytic activity. Moreover, a quantity of chloromethane was formed and ethylene could be produced through the dimerization of chloromethane, which was effective for improving the OCM catalytic activity of the Li/SnO_2 catalyst.

Acknowledgements This work was supported by the "Strategic Priority Research Program" of the Chinese Academy of Sciences (No. XDA09030101) and the Petro China Innovation Foundation (No. 2016D-5007-0506).

References

1. Keller GE, Bhasin MM (1982) J Catal 73:9–19
2. Lee J, Oyama S (1988) Catal Rev 30:249–280
3. Palermo A, Vazquez JPH, Lee A, Tikhov M, Lambert R (1998) J Catal 177:259–266
4. Machocki A, Jezior R (2008) Chem Eng J 137:643–652
5. Zheng W, Cheng DG, Chen FQ, Zhan XL (2010) J Nat Gas Chem 19:515–521

6. Park JH, Lee DW, Im SW, Lee YH, Suh DJ, Jun KW, Lee KY (2012) Fuel 94:433–439
7. Uzunoglu C, Leba A, Yildirim R (2017) Appl Catal A 547:22–29
8. Shubin A, Zilberberg I, Ismagilov I, Matus E, Kerzhentsev M, Ismagilov Z (2018) Mol Catal 445:307–315
9. Wang DZ, Wen SL, Chen J, Zhang SY, Li FQ (1994) Phys Rev B 49:14282–14285
10. Xie J, Chen L, Au CT, Yin SF (2015) Catal Commun 66:30–33
11. Goudarzi F, Izadbakhsh A (2017) Reac Kinet Mech Cat 121:539–553
12. Rorf J, Roos JA, Vertman LJ, Vanommen JG (1989) Appl Catal 56:119–135
13. Nibbelke RH, Scheerova J, Decroon MHJN, Marin GB (2010) J Catal 156:106–119
14. Lunsford JH, Hinson PG, Rosynek MP, Shi CL, Xu MT, Yang XM (1994) J Catal 147:301–310
15. Raouf F, Taghizadeh M, Yousefi M (2013) Reac Kinet Mech Cat 110:373–385
16. Wang DJ, Rosynek MP, Lunsford JH (1995) J Catal 151:155–167
17. Hong JH, Yoon KJ (2001) Appl Catal A 205:253–262
18. Hiyoshi N, Ikeda T (2015) Fuel Process Technol 133:29–34
19. Wang Y, Arandiyan H, Tahini HA, Scott J, Tan X, Dai HX, Gale JD, Rohl AL, Smith SC, Amal R (2017) Nat Commun 8:1–7
20. Song JJ, Sun YN, Ba RB, Huang SS, Zhao YH, Zhang J, Sun YH, Zhu Y (2015) Nanoscale 7:2260–2264
21. Choudhary VR, Rane VH (1994) J Chem Soc Faraday Trans 90:3357–3365
22. Kus S, Otremba M, Taniewski M (2003) Fuel 82:1331–1338
23. Hou YH, Han WC, Xia WS, Wan HL (2015) ACS Catal 5:1663–1674
24. Voskresenskaya EN, Roguleva VG, Anshits AG (1995) Catal Rev Sci Eng 37:101–143
25. Arandiyan H, Dai HX, Deng JG, Wang Y, Sun HY, Xie SH, Bai BY, Liu YX, Ji KM, Li JH (2014) J Phys Chem C 118:14913–14928
26. Arandiyan H, Scott J, Wang Y, Dai HX, Sun HY, Amal R (2016) ACS Appl Mater Interfaces 8:2457–2463
27. Wang X, Liu D, Li J, Zhen J, Zhang H (2015) NPG Asia Mater 7:e158
28. Chen J, Arandiyan H, Gao X, Li J (2015) Catal Surv Asia 19:140–171
29. Long RQ, Wan HL (1997) Appl Catal A 159:45–58
30. Huang P, Zhao YH, Zhang J, Zhu Y, Sun Y (2013) Nanoscale 5:10844–10848
31. Ding WP, Ding WP, Chen Y, Fu XC (1994) Catal Lett 23:69–78
32. Ferreira VJ, Tavares P, Figueiredo JL, Faria JL (2013) Catal Commun 42:50–53
33. Kang M, Park ED, Kim JM, Yie JE (2007) Appl Catal A 327:261–269
34. Peng XD, Richards DA, Stair PC (1990) J Catal 121:99–109
35. Lee MR, Park MJ, Jeon W, Choi JW, Suh YW, Suh DJ (2012) Fuel Process Technol 96:175–182
36. Sun J, Thybaut JW, Marin GB (2008) Catal Today 137:90–102
37. Fleischer V, Steuer R, Parishan S, Schomäcker R (2016) J Catal 341:91–103
38. Andersen PJ, Kung HH (1992) J Phys Chem 96:3114–3123
39. Delavari S, Amin NAS, Mazaheri H (2014) Reac Kinet Mech Cat 113:557–573
40. Osada Y, Koike S, Fukushima T, Ogasawara S (1990) Appl Catal 59:59–74
41. Dai HX, Ng CF, Au CT (1999) Catal Lett 57:115–120
42. Stranick MA, Moskwa A (1993) Surf Sci Spectra 2:45–49
43. Klingenberg B, Vannice MA (1996) Chem Mater 8:2755–2768
44. Aika K, Moriyama T, Takasaki N, Iwamatsu E (1986) J Chem Soc Chem Commun 18:1210–1211
45. Xu XL, Liu F, Han X, Wu YY, Liu WM, Zhang RB, Zhang N, Wang X (2016) Catal Sci Technol 6:5280–5291
46. Sun GB, Hidajat K, Wu XS, Kawi S (2008) Appl Catal B 81:303–312
47. Wu X, Kawi S (2009) Catal Today 148:251–259
48. Wu X, Kawi S (2010) Cryst Growth Des 10:1833–1841
49. Shiow SL, Chun LC, Dong JC, Chia CC (2002) Water Res 36:3009–3014
50. Rani RS, Lakshmanan A (2016) J Lumin 174:63–69
51. Ohtsuka Y, Kuwabara M, Tomita A (1989) Appl Catal 47:307–315